Physical controls and predictability of stream hyporheic flow evaluated with a multiscale model

Susa H. Stonedahl,[1,2] Judson W. Harvey,[3] Joel Detty,[3,4] Antoine Aubeneau,[1] and Aaron I. Packman[1]

Received 7 November 2011; revised 21 August 2012; accepted 27 August 2012; published 6 October 2012.

[1] Improved predictions of hyporheic exchange based on easily measured physical variables are needed to improve assessment of solute transport and reaction processes in watersheds. Here we compare physically based model predictions for an Indiana stream with stream tracer results interpreted using the Transient Storage Model (TSM). We parameterized the physically based, Multiscale Model (MSM) of stream-groundwater interactions with measured stream planform and discharge, stream velocity, streambed hydraulic conductivity and porosity, and topography of the streambed at distinct spatial scales (i.e., ripple, bar, and reach scales). We predicted hyporheic exchange fluxes and hyporheic residence times using the MSM. A Continuous Time Random Walk (CTRW) model was used to convert the MSM output into predictions of in stream solute transport, which we compared with field observations and TSM parameters obtained by fitting solute transport data. MSM simulations indicated that surface-subsurface exchange through smaller topographic features such as ripples was much faster than exchange through larger topographic features such as bars. However, hyporheic exchange varies nonlinearly with groundwater discharge owing to interactions between flows induced at different topographic scales. MSM simulations showed that groundwater discharge significantly decreased both the volume of water entering the subsurface and the time it spent in the subsurface. The MSM also characterized longer timescales of exchange than were observed by the tracer-injection approach. The tracer data, and corresponding TSM fits, were limited by tracer measurement sensitivity and uncertainty in estimates of background tracer concentrations. Our results indicate that rates and patterns of hyporheic exchange are strongly influenced by a continuum of surface-subsurface hydrologic interactions over a wide range of spatial and temporal scales rather than discrete processes.

Citation: Stonedahl, S. H., J. W. Harvey, J. Detty, A. Aubeneau, and A. I. Packman (2012), Physical controls and predictability of stream hyporheic flow evaluated with a multiscale model, *Water Resour. Res.*, *48*, W10513, doi:10.1029/2011WR011582.

1. Introduction

[2] Surface water continually exchanges with groundwater in lotic systems, and temporary routing of stream water throughflow paths beneath and adjacent to streams is referred to as hyporheic flow [*Williams and Hynes*, 1974; *Harvey and Bencala*, 1993; *Packman and Bencala*, 2000]. Streambed sediments generally have high microbial biomass and diversity, making the hyporheic zone a biologically rich transition area between groundwater and surface water that influences the fate of a variety of water-borne substances, including organic carbon, nutrients, and many pollutants. Measuring and modeling hyporheic exchange in natural systems is therefore critical to predicting contaminant transport and fate [*Benner et al.*, 1995; *Fuller and Harvey*, 2000; *McKnight et al.*, 2001; *Medina et al.*, 2002], nutrient depletion and availability [*Stream Solute Workshop*, 1990; *Triska et al.*, 1993; *Valett et al.*, 1996], and downstream changes in water quality [*Mulholland et al.*, 1997; *Jones and Mulholland*, 2000].

[3] Tracer-injection experiments are often used to characterize transport in individual stream reaches through measurements of solute concentrations downstream of an injection site [*Bencala and Walters*, 1983; *Stream Solute Workshop*, 1990]. Several models, and notably the Transient Storage Model (TSM), are used to interpret exchange processes with surface and subsurface storage zones based on inverse modeling of such solute tracers [*Bencala and Walters*, 1983; *Choi et al.*, 2000; *Boano et al.*, 2007; *Neilson et al.*, 2010]. However, inverse modeling of stream tracers cannot necessarily identify specific locations of storage or associated exchange fluxes [*Briggs et al.*, 2009;

[1]Department of Civil and Environmental Engineering, Northwestern University, Evanston, Illinois, USA.
[2]Now at the Engineering and Physics Department, St. Ambrose University, Davenport, Iowa, USA.
[3]U.S. Geological Survey, Reston, Virginia, USA.
[4]Now at Normandeau Associates, Inc., Bedford, New Hampshire, USA.

Corresponding author: A. I. Packman, Northwestern University, 2145 Sheridan Road, Tech A314, Evanston, IL 60208-3109, USA. (a-packman@northwestern.edu)

0043-1397/12/2011WR011582

Choi et al., 2000]. Also, inverse modeling is often constrained by an assumed formulation for storage, e.g., the exponential residence time function implicit in the TSM. Furthermore, tracer-based measurements are time-consuming, expensive, and difficult to generalize for different streams or even different flows in the same stream. The lack of general, process-based theory makes it very difficult to transfer results from one study to other locations or even to different flow conditions in the same channel [*Salehin et al.*, 2003; *Harvey et al.*, 2003]. As a result, previous predictions of storage-exchange in streams are largely based on empirical relationships between parameters from stream tracer experiments and simple physical measurements such as friction factor [*Harvey and Wagner*, 2000]. Specific predictions of hyporheic flow are possible based on scaling relationships of the hydraulic forces that drive hyporheic flow and the flow resistance of the sediment [*Grant and Marusic*, 2011; *O'Connor and Harvey*, 2008]; however, these scaling relationships are primarily based on laboratory flume data and therefore cannot account for interactions across the diverse topographic scales that occur in natural rivers. Consequently, detailed predictions of storage-exchange processes in streams is thought to be limited [*Beven and Binley*, 1992], which has implications for how streams can be better managed, e.g., through improved design of restorations [*O'Connor et al.*, 2010].

[4] Physically based models of hyporheic flow can incorporate scales of stream topography ranging from small bedforms that scale with the stream depth (dunes) [*Thibodeaux and Boyle*, 1987; *Elliott and Brooks*, 1997; *Boano et al.*, 2009; *Cardenas et al.*, 2009b] to larger features that scale with the river width such as bars and riffles [*Harvey and Bencala*, 1993; *Gooseff et al.*, 2003], up to bank undulations and meanders that scale with valley width [*Wroblicky et al.* 1998; *Larkin and Sharp*, 1992]. Prior investigations have generally focused on specific spatial scales, so little is currently known about the interactions in rates and patterns of hyporheic exchange across scales. For example, computational fluid dynamics (CFD) models provide an appealing choice for simulating hyporheic exchange at the spatial scale of small morphological features (e.g., dunes, ripples, woody debris) [*Elliott and Brooks*, 1997; *Packman and Brooks*, 2001; *Cardenas and Wilson*, 2007; *Cardenas*, 2009a; *Boano et al.*, 2009]. In contrast, hydrogeologic models are typically applied at the scale of relatively large topographic features such as bars or meanders up to the scale of entire stream reaches [*Wondzell and Swanson*, 1996; *Harvey and Bencala*, 1993; *Storey et al.*, 2003]. All of these models are useful for determining the effects of features at the discrete scales being considered. However, they do not capture the full complexity as a result of limitations imposed by factors such as the resolution and spatial extent of topographic measurements and model simulations.

[5] A predictive modeling approach that is physically based, three-dimensional, and computationally efficient is highly desirable. Computational cost makes it infeasible to develop a purely process-based model for broad multiscale application, but an approximate model would still be extremely useful to account for effects of stream planform, variable flow conditions and channel morphology, and sediment hydrogeology [*Wörman et al.*, 2007; *Cardenas*, 2009b; *Stonedahl et al.*, 2010]. Here we adapt the three-dimensional MSM that we previously applied to flume experiments in *Stonedahl et al.* [2010] to simulate hyporheic flow for the field conditions at Sugar Creek. This MSM is a physically based model of stream-groundwater interactions that represents the effects of a wide range of topographic features but is also practical for field applications at the reach scale. Unlike the TSM, this model predicts hyporheic flow independently of solute tracer data. Using basic physical measurements of stream properties, it predicts hyporheic exchange fluxes and timescales and also can be used to partition components of hyporheic flow associated with various scales of streambed topography from small ripple bedforms up to meanders. It simulates three-dimensional exchange including both the flow directly beneath the streambed and the lateral hyporheic zone on both sides of the stream.

[6] The MSM is based on understanding that surface-groundwater interactions are induced by topographic variations over many spatial scales [*Wörman et al.*, 2007; *Cardenas*, 2008]. We used the model here to examine the relative importance of physical controls on hyporheic flow and also to evaluate the merits of a physically based model relative to traditional stream tracer experimentation and inverse modeling using the TSM. Here we use the MSM to predict hyporheic exchange flow paths, evaluate the interaction between flows induced at different scales, and characterize the patterns and fluxes that influence in stream solute dynamics. This represents the first application of such a MSM to a natural stream. We also integrate the MSM with a Continuous-Time Random Walk (CTRW) model to predict downstream solute transport, and compare the results with measured tracer transport and TSM fits. We then evaluate the range of processes that are adequately captured using each method. Finally, we exploit the predictive capability of MSM to investigate interactions between changing groundwater levels surrounding the stream on fluxes and patterns of hyporheic exchange beneath large and small-scale topographic features. The results indicate that the more detailed information on interactions across scales encapsulated in the MSM supports better predictions of hyporheic flux, subsurface residence times and its effects on downstream solute transport.

2. Methods

2.1. Solute Tracer Experiment and Physical Measurements in an Agricultural Stream

2.1.1. Field Site Description

[7] Our field measurements were made in Sugar Creek: a small gravel bed stream near Kentland, IN that has been ditched and straightened to promote drainage from adjacent agricultural fields. This stream was studied previously to understand the processing of nitrogen in small agricultural streams [*Böhlke et al.*, 2009; *Tobias et al.*, 2007; *Böhlke et al.*, 2004; *Smith et al.*, 2006]. Our investigation directly supports these studies by characterizing hyporheic transport of solutes and the timescales of hyporheic flow where key reactions such as denitrification occur. Sugar Creek is a stream of intermediate complexity (Figure 1) where incision and mass wasting from the banks has created a relatively straight channel with widely spaced pools and riffles. Incision occurred through a layer of gravel, pebble, and coarse sandy glacial sediments that now compose the streambed.

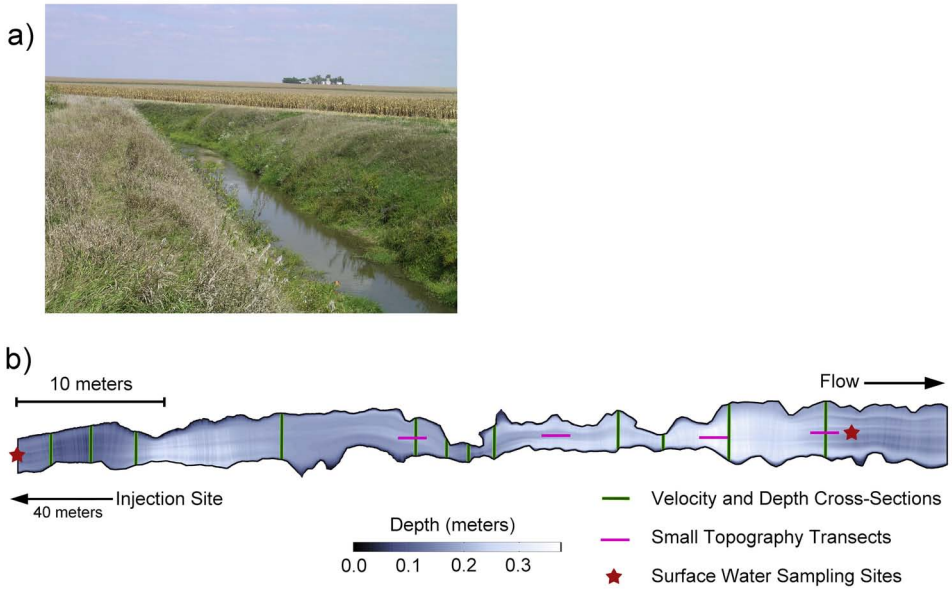

Figure 1. Sugar Creek, a straightened and ditched agricultural stream in Northwest Indiana. (a) Site overview. (b) Map of study reach indicating channel planform, bathymetry, and observation locations.

The stream is underlain by a continuous layer of very fine silt, which produces an essentially impermeable boundary at approximately 0.28 m beneath the stream channel.

2.1.2. Site Characterization

[8] The stream planform was mapped using 13 oblique digital photographs taken from the top of the bank. Each photograph contained a surveyor's rod laid horizontally along the stream, which we used to rectify the sequence of images into a continuous map of the reach. The stream width was measured at multiple cross-sections that had been flagged to be observable in photographs. Observation locations are shown in Figure 1. The stream had a mean width of 2.1 $\pm$ a standard error of 0.9 m. We measured water surface elevations to calculate the valley slope of the water surface, S_v, which we assumed was equal to the slope of the impermeable layer beneath the stream. These measurements were made relative to a mounted surveying level at 14 points near the center of the stream to 0.001 m precision. Then we calculated the average valley slope of the water surface, 9.7×10^{-4}, from these measurements.

[9] We measured stream velocity and depth on 12 cross-sections, as shown in Figure 1. We calculated the average maximum depth of the cross-sections to be 0.16 $\pm$ 0.05 m. Cross-sections had tighter spacing around the flow constriction formed by a bank slump near the middle of the reach. Velocities and depths were measured on a 0.5 or 1.0 ft spacing, depending on the stream width. Stream depths and planform were later used to characterize bar topography. At each location that depth was measured, the mean stream velocity was estimated by measuring the local velocity at 6/10ths of the depth using a Sontek FlowTracker Handheld Acoustic Doppler Velocimeter (ADV). The average volumetric discharge was very stable at Sugar Creek during the injection, varying only a few percent, i.e., 0.040 $\pm$ 0.001 $m^3\ s^{-1}$.

[10] We also measured the fine-scale topography of the streambed. The mixed grain sizes ranging from sand to cobbles prevented formation of highly regular ripples or dunes, and instead the bed had a variety of centimeter-scale roughness features. This scale of topography is not typically considered in field observations of solute transport, but is expected to significantly influence hyporheic exchange based on prior analyses of advective pore water flow induced by bottom roughness. To resolve this topography, we surveyed the bed along four 2-m long transects using a Leica Disto Proa laser rangefinder mounted to slide across a level bar, which was in turn mounted on two surveying tripods. For each transect, bed elevations were measured at 5-cm intervals over a 2-m distance. The rangefinder uses a red LED light source, requiring shallow water and good visibility for observation of bed surface topography. Fish, surface waves and other reflections interfere with the measurements. To reduce these adverse effects, we mounted the rangefinder within a partially submerged clear plastic cylinder. The cylinder minimized interference by reducing the depth of water and smoothing the water interface. We constructed the cylinder bottom with an inclined face to shed bubbles and suspended objects around the measurement location. Elevation measurements were calibrated by floating a piece of paper on the water under the rangefinder. Measurements were made in triplicate.

[11] We collected nine cores to characterize the bed sediment size distribution and porosity. Cores were obtained using plastic cylinders having 0.048 m nominal inner diameter and ranging between 0.1 and 0.3 m in length. Cores were extruded and sectioned in the field, and dried and weighed in the laboratory. Grain size was determined by dry sieving and ranged from 0.062 to 41 mm with an average median grain size in cores of 3.2 mm, an average d_{10} of 0.43 mm, and an average porosity of 0.43. To determine sediment hydraulic conductivity, K, we performed several field permeameter tests using large (30 cm diameter) cylinders whose walls had been beveled on one end and pushed into the sediment to a depth of 0.1 m. A constant head test was conducted by pumping stream water continuously into

the cylinders and monitoring the head until it stabilized [*Reynolds et al.*, 2002; *Landon et al.*, 2001; *Hvorslev*, 1951]. The mean of several repeated tests in two cylinders was 0.063 ± 0.01 cm s^{-1}. We used the mean hydraulic conductivity as a constant value in our MSM simulations.

2.1.3. Solute Tracer Injection

[12] A 177 liter solution of potassium bromide (KBr) in filtered stream water was prepared on the site in a large plastic container. The injection solution had a bromide concentration of 151 g L^{-1}, and we injected this at a rate of 0.155 L min^{-1} into the stream for a period of 19 h beginning at 1800 UTC on 12 September 2004. Stream water samples were collected for tracer analysis on planned intervals beginning just prior to the tracer injection and lasting for 50 h. All water sampling was undertaken at endpoints of the experimental reach, at a spacing of 52 m. The stream appeared to be well mixed at these locations. Near the times when tracer concentrations changed rapidly (i.e., when the injection started and when it stopped) the samples were collected by hand on a 30-s sampling schedule. The frequency of hand sampling was relaxed over time until it eventually matched the 30-min sampling schedule that had been preset for automatic water samplers. Unfiltered subsamples from each well mixed sample were transferred into prelabeled 20-ml plastic vials and stored at ambient temperature. In addition, a 5-L carboy of stream water was collected upstream of the injection site for analysis of the bromide background concentration in Sugar Creek. At the conclusion of the experiment, the carboy and approximately 300 individual samples were transported to the laboratory for analysis of bromide concentration using ion chromatography. Aliquots of each sample were individually filtered when they were prepared for analysis. Our setup had a detection limit for bromide of 0.01 mg L^{-1}. The solute tracer experiment provided the data needed to estimate streamflow discharge based on dilution gauging at the endpoints of the experimental reach. From these data the average net groundwater discharge to the stream reach was calculated by difference. Our velocity gauging data, when compared to dilution gauging flow estimates [*Harvey and Wagner*, 2000], indicated that losses were insignificant, which is consistent with modified agricultural streams that were specifically dug down to drain the surrounding landscape.

2.2. Theory and Modeling

2.2.1. Reach-Scale Tracer Modeling Using the TSM

[13] We used two very different modeling approaches to analyze solute transport in Sugar Creek: inverse modeling of solute tracer data using the TSM, and our physically based MSM-CTRW approach. It is essential to understand the processes represented by each model. We used the TSM to estimate parameters that characterize advection, longitudinal dispersion, groundwater inflow, and transient storage in the study reach. In the TSM, storage is represented as mass transfer with a hypothetical well-mixed storage zone. The storage zone is assumed to have a constant size, characterized by A_s, and exchange rate, characterized by a mass transfer coefficient, α. Note that the assumption of mass transfer with a well-mixed storage zone yields an exponential residence time distribution, so $1/\alpha$ is also a first-order exchange timescale.

[14] We used an extended version of the TSM, the OTIS-2stor model, which includes two different (but still exponentially distributed) distributions of water residence times [*Choi et al.*, 2000; *Harvey et al.*, 2005]. The governing equations of the OTIS-2stor model are

$$\frac{\partial C}{\partial t} = -\frac{Q}{A}\frac{\partial C}{\partial x} + \frac{1}{A}\frac{\partial}{\partial x}\left(AD_L\frac{\partial C}{\partial x}\right) + \frac{q_L^{in}}{A}(C_L - C) + \alpha_1(C_{S1} - C) + \alpha_2(C_{S2} - C) \tag{1}$$

$$\frac{dC_{S1}}{dt} = \alpha_1\frac{A}{A_{S1}}(C - C_{S1}) \tag{2}$$

$$\frac{dC_{S2}}{dt} = \alpha_2\frac{A}{A_{S2}}(C - C_{S2}) \tag{3}$$

where t is time (s) and x is downstream distance (m); C, C_L, C_{S1}, and C_{S2} are the solute concentration (mg L^{-1}) in the main channel, lateral inflow, storage zone 1, and storage zone 2, respectively; Q is the volumetric flowrate (m^3 s^{-1}); A, A_{S1} and A_{S2} are the cross-sectional area (m^2) in the main flow zone, storage zone 1, and storage zone 2, respectively; D_L is the longitudinal dispersion coefficient (m^2 s^{-1}); q_L^{in} is the lateral inflow rate ((m^3 s^{-1})/m); α_1 and α_2 are storage zone exchange coefficients (s^{-1}). OTIS-2stor is similar to formulations of the TSM by *Briggs et al.* [2009] and *Neilson et al.* [2010]. Our approach to parameter estimation follows standard techniques [e.g., *Harvey and Wagner*, 2000] that begin with direct calculation from tracer data of the volumetric flowrate of surface water in the channel (Q) and the inflow flux (q_L^{in}) estimated using measurements of (1) injection pumping rate, (2) Br concentration in the injection solution barrel, (3) background concentration of Br tracer, and (4) concentrations of Br in surface water during the injection at a downstream monitoring location. We assumed that there was no lateral outflow. To estimate the other model parameters that best describe the tracer data, we used the USGS numerical code OTIS-P [*Runkel*, 1998] with its associated parameter optimization code that we extended for two storage zones. The optimized parameters included the geometric properties A, A_{S1}, and A_{S2}, the in stream dispersion coefficient D_L, and the exchange coefficients α_1 and α_2.

[15] The OTIS-P optimization seeks to separate mixing associated with dispersion and transient storage, as indicated in equation (1). Longitudinal mixing processes that achieve equilibrium (i.e., wherein the tracer experiences the full range of longitudinal velocities in the experimental reach) are characterized as longitudinal dispersion [*Fischer et al.*, 1979]. This is generally referred to as regular advection-dispersion behavior, or Taylor dispersion [after *Taylor*, 1953], and is described by the advection-dispersion equation (ADE). In regular dispersion, the variance of the breakthrough curve increases linearly with travel time and in proportion to the dispersion coefficient. Some travel distance is always required to achieve equilibrium over the velocity profile. Before this distance is achieved, the variance increases nonlinearly with time and the concentration distribution can be asymmetric in space [*Fischer et al.*, 1979]. This preasymptotic dispersion is normally addressed in field injections

by allowing the tracer to become well-mixed over the channel cross-section in a designated mixing reach located upstream of the region of primary measurements. Here we used a mixing reach of 40 m between the injection location and the upstream end of the observation reach. The TSM represents extended preasymptotic tailing associated with finite storage zones that are not well-mixed with the active stream channel at the scale of the study reach. Typically TSM fits yield stream areas smaller than measured cross-sections, implying that stagnant or slowly flowing regions within the stream channel are represented by the transient storage terms instead of stream transport terms. Further, the tails represented by the TSM are transient by definition, and will eventually decay as the solute becomes mixed between the water column and storage zones.

[16] More recently, it has been recognized that there are some cases that never converge to Taylor dispersion, and for which the advection-dispersion equation is not a suitable model. Extremely wide velocity distributions make it impossible to achieve equilibrium, and do not produce Gaussian breakthrough curves for any travel distance. In this case, the concentration distribution becomes progressively more skewed. This behavior has been referred to in the physics and geophysics literature as anomalous diffusion (or dispersion), and breakthrough curves having skewness that persists or grows over time are referred to as heavy-tailed [*Metzler and Klefter*, 2000; *Schumer et al.*, 2003; *Berkowitz et al.*, 2006]. A major open question is whether solute transport in rivers generally follows regular dispersion behavior, for which the ADE and TSM are appropriate models, or anomalous dispersion behavior, for which other models are needed. We explore this here by comparing TSM fits with alternative model formulations based on the MSM and CTRW, as described in section 2.2.2.

2.2.2. MSM of Groundwater and Surface Water Interactions

[17] The MSM employs a spectral scaling approach as the basis for analyzing topography-induced exchange between surface and subsurface water in streams. We calculate the head at the stream channel boundaries as a function of the stream channel topography using an extension of the two-dimensional bed form model presented by *Elliott and Brooks* [1997]. First, the stream channel is straightened using a conformal mapping in order to roughly align streamflow with the longitudinal axis of the orthogonal domain, and then the straightened topography is scaled according to local system characteristics and decomposed using Fourier analysis into spectral components. The resulting head distribution over the stream channel surface is then used as a boundary condition to calculate the subsurface flow field using a finite difference approach. The model is presented in greater detail and applied to the case of hyporheic exchange within a meandering channel in a laboratory flume in *Stonedahl et al.* [2010]. Here we extend the model to account for the additional complexity inherent to natural streams. The extended version accommodates larger stream reaches with more complex topography, utilizes available (limited) field data instead of high-resolution laboratory data, and includes interactions with larger-scale groundwater flows that create gaining or losing conditions over the reach.

2.2.2.1. Generation of the Topographic Surface

[18] We used the planform determined by photography and depth profiles along each cross-section (section 2.1.1) to generate a function for the stream planform topography, as shown in Figure 1. We then transformed the channel outline into a rectilinear space with a Schwarz-Christoffel conformal mapping [*Driscoll*, 1996; *Stonedahl et al.*, 2010]. Within this transformed space, stream cross-sections are all parallel to each other and perpendicular to the banks. The raw data for each cross-section were interpolated using the piecewise cubic Hermite interpolation (MATLAB interp1 function over the ξ-coordinate) and placed in this rectilinear space according to its downstream distance (Figure 2). Then we used the interpolation function again to determine points in between the cross-sections in the transformed domain. Figure 2 shows the resulting channel bathymetry in both the orthogonal space (ξ, η) and transformed back onto natural coordinates (x, y).

[19] We characterized the streambed roughness along four fine-resolution topographic transects. In order to generalize the limited observations of fine topography from the four longitudinal transects to the full domain, we constructed a synthetic 1-D streambed elevation profile by randomly assigning the elevation profile of one of the observed transects to all areas where topography was not measured. In other words, the small streambed surface topography throughout the reach consists of a random tiling of the four fine-resolution transect datasets. We then fit a 1-D Fourier series to the synthetic 1-D elevation profile and converted this to 2-D over the entire streambed by scaling each elevation according to its distance from the stream banks:

$$T_{S3}(\xi,\eta) = T_{S2}(\xi)\cdot\frac{d(\xi,\eta)}{d} \tag{4}$$

where $T_{S3}(\xi,\eta)$ is the 2-D elevation distribution for small topography in the orthogonal space, $T_{S2}(\xi)$ is the 1-D elevation profile for small topography, $d(\xi,\eta)$ is the local water

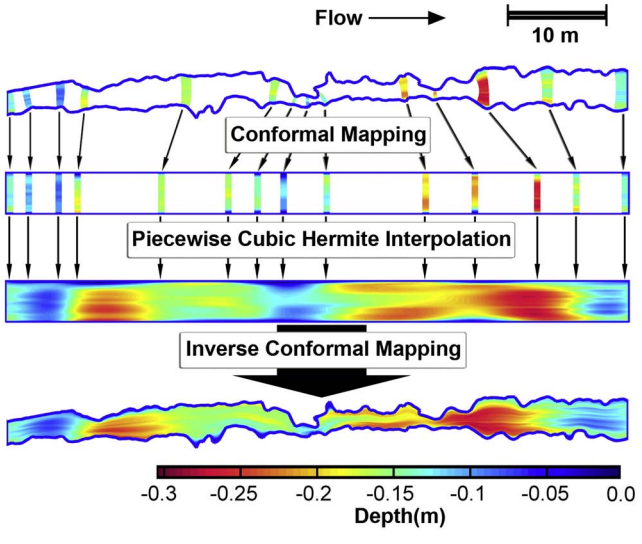

Figure 2. Steps used to generate map of large-scale channel bathymetry from local observations.

depth in the orthogonal space, d is the average depth of the stream calculated from the four transects, η is the distance across the stream within the conformal domain, and ξ is the distance downstream within the conformal domain. The complete topography function of the stream, $T(x,y)$, was calculated by superimposing $T_{S3}(\xi,\eta)$ onto $T_L(\xi,\eta)$, the large-scale stream bathymetry in the orthogonal space (shown in Figure 2), and transforming the result back into the real domain.

2.2.2.2. Calculation of Head Distribution Over the Stream Channel Boundary

[20] Head variations associated with the large-scale stream bathymetry (Figure 3) and small-scale bed surface topography were calculated separately. First, the gravitational head was applied on the entire streambed surface using the equation $S_s\xi$ in the orthogonal domain. Velocity head perturbations due to flow over small topography were calculated using the method presented in *Stonedahl et al.* [2010]. The velocity head distribution over the bed surface was calculated by multiplying the elevation of small topography at each point, $T_{S3}(\xi,\eta)$, by the scaling factor $h'_m(\xi,\eta)$:

$$h'_m(\xi,\eta) = \frac{0.28\left(\frac{V(\xi,\eta)^2}{2g}\right)}{\sqrt{2}\sigma_H(\xi)} \begin{cases} \left(\frac{2\sqrt{2}\sigma_H(\xi)/d(\xi)}{0.34}\right)^{3/8} & 2\sqrt{2}\sigma_H(\xi)/d(\xi) \le 0.34 \\ \left(\frac{2\sqrt{2}\sigma_H(\xi)/d(\xi)}{0.34}\right)^{3/2} & 2\sqrt{2}\sigma_H(\xi)/d(\xi) \ge 0.34 \end{cases} \quad (5)$$

where $V(\xi,\eta)$ is the stream velocity, which varies in both the longitudinal and transverse directions within the channel, g is the gravitational constant, $\sigma_H(\xi)$ is the standard deviation of bed surface elevation in each cross-section, defined as $\sigma_H(\xi) = \sigma_T d(\xi)/d$, where d and σ_T are the mean and standard deviation of depth in the four small topography transects, respectively, and $d(\xi)$ is the mean stream depth at each cross-section, excluding banks (operationally, $d(\xi)$ was taken as the mean depth of the middle half of the stream at each location, ξ). We assumed that the volumetric discharge (0.04 m^3 s^{-1}) increased with downstream distance at a constant rate estimated from the tracer as the groundwater discharge per stream length. As described in *Stonedahl et al.* [2010], we assumed that the maximum velocity follows the thalweg and the velocity reaches 0 at the banks. Then the orthogonal grid, $T'_{S3}(\xi,\eta)$, where $T'_{S3}(\xi,\eta) = h'_m(\xi,\eta) * T_{S3}(\xi,\eta)$ was fit with a Fourier function and each wavelength in the ξ direction is shifted by a quarter of a wavelength upstream to produce a function for head in the conformal domain, $H(\xi,\eta)$. This [1/4] wavelength shift produces higher head on the upstream sides of bedforms, as observed for a single bed form by *Fehlman* [1985].

2.2.2.3. Three-Dimensional Simulation of Subsurface Flow

[21] Subsurface flow was simulated using the finite difference model, MODFLOW 2000 [*Harbaugh et al.*, 2000], as described in *Stonedahl et al.* [2010]. The top boundary of the groundwater flow simulation was taken as the stream bathymetry inside of the stream channel and the water table outside of the stream channel. The lateral, downstream, and bottom boundaries were planes. The upstream, downstream, stream channel, and lateral boundaries were applied with constant-head boundary conditions, while the bottom boundary was applied with a no-flux boundary condition to simulate the effect of the subsurface clay layer. The bottom boundary had a slope equal to the water surface and was located 0.28 m below the deepest part of the stream. The domain width was eight times the maximum stream width. Simulations with a domain width of six times the stream width yielded a negligible difference in results, thus assuring that the domain width was sufficiently large enough to avoid lateral boundary effects.

[22] The groundwater system was simulated with a constant longitudinal head gradient equal to the stream valley

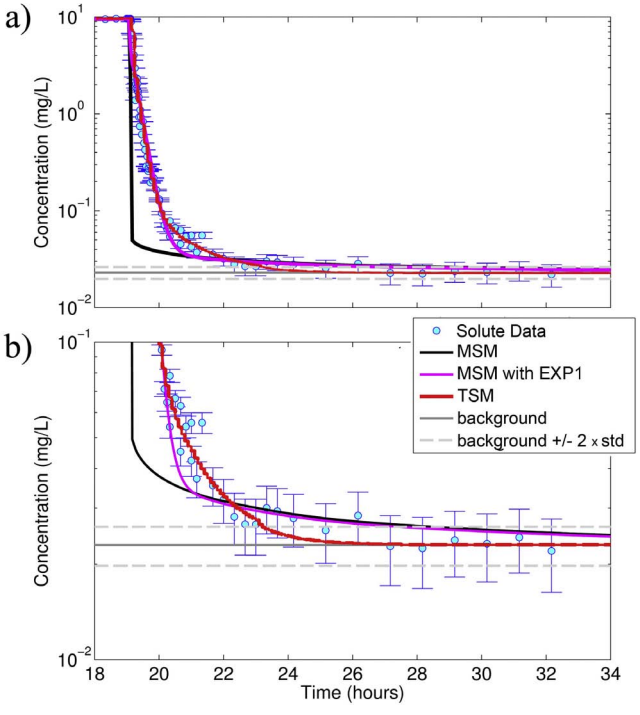

Figure 3. Breakthrough curves showing extended tails of solute tracer concentrations measured at the downstream sampling site after the shut off of the tracer injection. Shown in comparison are the solute tracer data, a priori MSM simulations (with and without an exponential term to account for fast storage-exchange), and the TSM (OTIS-2Stor). Note that the tracer injection lasted 19 h. (a) Measured solute concentrations are denoted by cyan circles with errors bars showing the 95% confidence bands (twice the standard deviation). The MSM prediction is shown by a black line. The magenta line indicates results of the MSM predictions including an additional fast exponential exchange process fitted with the CTRW model to the early time tailing data. (b) An expanded view of the comparison between solute data, a priori predictions of the multiscale model, and the inversely estimated results of an OTIS-2Stor TSM. The multiscale model predicts longer timescale storage compared with the TSM model, but at late times both models produce simulations that fall within the uncertainty bounds of the solute tracer data.

slope S_v. For each imposed groundwater inflow, the water table between the lateral boundaries of the simulation domain and the stream channel was calculated using a 2-D MODFLOW simulation for an unconfined aquifer based on the distribution of head along the stream channel boundaries from the MSM and the appropriate groundwater levels along the domain boundaries. The resulting head distribution was then used to construct an equivalent 3-D groundwater domain for each case, so that the interaction of groundwater and hyporheic exchange flows could be simulated in 3-D. In order to investigate interactions between groundwater discharge and hyporheic flow, we imposed higher groundwater levels at the lateral boundaries of the simulation domain to control the discharge of groundwater to the stream. Simulations were first performed with the boundary head set to match the tracer-observed groundwater discharge to the stream, and then the extent of groundwater inflow was varied to examine interactions between groundwater discharge and hyporheic exchange.

[23] The computer memory needed to simulate 3-D groundwater flow with the resolution used to characterize small topographic features in the stream was significantly larger than MODFLOW's 2GB size limitation. In order to circumvent this limitation, we first calculated the 3-D head distribution throughout the domain on a coarse grid, and then ran multiple simulations along the stream using a fine grid with the coarse grid values imposed as boundary conditions. For the three-dimensional simulation, the coarse grid had dimensions of 1001 × 584 × 17 (longitudinal × lateral × vertical) nodes with a horizontal spacing of 0.0625 m. The fine grid had dimensions of 5001 × 576 × 17 nodes with a horizontal spacing of 0.0125 m. Both grids had a higher density of layers near the surface in order to better resolve shallow hyporheic exchange flow paths. The top layer was 0.0002 m thick, the bottom layer was 0.002 m thick, and the intermediate layers increased in thickness by a factor of 1.5.

[24] The velocity field was calculated from the head distribution using Darcy's law, $q_s = -K\nabla h_1(x,y,z)$, where q_s is the specific discharge and K is the hydraulic conductivity. In spite of variations in the sediment at Sugar Creek, we treated the permeability as homogeneous, as no data were available to evaluate the spatial structure of permeability. Flux across the stream channel boundary, q_{int}, was calculated as $q_{\text{int}} = \hat{n} \cdot q_s$, where q_s is the local value of the Darcy velocity and $\hat{n}$ is the unit-normal to the surface, which was obtained from the topography function. The Darcy velocity was converted into the seepage or pore water velocity, q_p, using $q_p = q_s/\theta$, where θ is the porosity. A particle-tracking routine was used to determine subsurface flow paths and residence times from the simulated pore water velocity fields, as described in *Stonedahl et al.* [2010]. The initial particle placement was weighted by the interfacial boundary flux, and the particle tracking calculation was performed with constant distance step of 0.001 m. 1000 particles were tracked through the system.

2.2.3. CTRW Model for Generating Breakthrough Curves From Boundary Exchange Fluxes and Residence Time Distributions

[25] We used a Continuous Time Random Walk (CTRW) formulation [*Montroll and Weiss*, 1965; *Metzler and Klafter*, 2000; *Berkowitz et al.*, 2006; *Boano et al.*, 2007] to convert the MSM predictions of hyporheic flow into solute breakthrough curves that can be directly compared with the solute tracer data. The CTRW is a stochastic model that can encompass a wide range of transport timescales. Here it is used essentially as a generalized form of the TSM to provide greater flexibility for modeling a broad range of hyporheic residence time distributions. The evolution of the in stream tracer concentration is given by:

$$\frac{\partial C(x,t)}{\partial t} = \int_o^t M(t-t')[-U_\psi \frac{\partial C(x,t')}{\partial t} + K_\psi \frac{\partial^2 C(x,t')}{\partial x^2}]dt' \quad (6)$$

where M is a memory function that depends only on the residence time distribution, U_ψ and K_ψ are the in stream velocity and dispersion coefficient, respectively, corresponding to the first and second moments of the lumped distribution governing fluid motion in the stream [*Berkowitz et al.*, 2006]. Any formulation can be used for the memory function, allowing the CTRW model to represent a wide array of in stream and subsurface transport processes. Here we used the memory function described by:

$$\tilde{M}(u) = u\bar{t}\frac{\tilde{\psi}(u)}{1-\tilde{\psi}(u)} \quad (7)$$

where $\sim$ indicates the Laplace transformed expression, u is the Laplace variable, $\bar{t}$, is the mean time spent in the channel (x/U where x = reach length and U = average velocity), and ψ is the lumped residence time distribution describing the travel times downstream for the entire domain:

$$\tilde{\psi}(u) = \tilde{\psi}_o[u + \Lambda_1 - \Lambda_1\tilde{\phi}_1(u) + \Lambda_2 + \Lambda_2\tilde{\phi}_2(u)] \quad (8)$$

where ψ_o is the RTD in the active channel, described by a Gaussian with mean x/U and variance 2Kt, ϕ_1 is the RTD for in stream transient storage, Λ_1 is the exchange rate between the active channel and in stream storage zones, ϕ_2 is the RTD in the hyporheic zone and Λ_2 is the exchange rate between the main channel and the hyporheic zone. The CTRW approximates the TSM when exponential residence time distributions are used to represent surface and/or subsurface storage [*Dentz et al.*, 2003, Appendix C]. In the case of exponential ϕ_1 and ϕ_2, this is approximately equivalent to the TSM 2-STOR model presented in 2.2.1, with $\Lambda_1 = \alpha_1$ and $\Lambda_2 = \alpha_2$ and the mean of the exponential RTD corresponding to $A_S/A\alpha$. Alternatively, nonexponential storage terms can be considered for both surface and subsurface storage, including ones that will yield anomalous transport. For instance the memory function can be selected to simulate very broad subsurface residence time distributions, such as the heavy power law tails that have been observed in the field [*Haggerty et al.*, 2002; *Gooseff et al.*, 2003; *Cardenas et al.*, 2008].

[26] We used the CTRW model in two ways. First, we used it to predict solute transport along the study reach using MSM predictions of Λ_2 and ϕ_2. In this case, we obtained the parameter Λ_2 (the hyporheic exchange rate) as the boundary exchange flux predicted by the MSM normalized by the stream depth [as in *Boano et al.*, 2007]. The parameter ϕ_2, the hyporheic residence time distribution, was

taken directly as the Laplace transform of the RTD predicted by the MSM. Second, in a separate set of simulations, we added an additional fast exponential exchange process to represent in stream transient storage with the parameters Λ_1 and ϕ_1 taken from TSM fits.

[27] The breakthrough curve was calculated in two steps. First, we obtained a solution for a unit reach length and unit pulse input with the Dirichlet condition applied on the upstream boundary and the Neuman condition on the downstream boundary. This normalized solution, commonly referred to as the Green's function solution, was then convolved with the observed, normalized concentration-time history at the upstream boundary to obtain the breakthrough curve at the downstream end of the study reach. The inverse Laplace transform was performed using De Hoog's algorithm [*De Hoog et al.*, 1982]. We then calculated the in stream break through curve (BTC) using a modified form of the CTRW toolbox [*Cortis and Berkowitz*, 2005]. We expanded this software package to include two storage zones and to use arbitrary RTDs. The latter was necessary to incorporate the RTDs predicted by the MSM. As a quality control, we replicated the OTIS 2-STOR model with our CTRW code using two exponential storage zones and found virtually indistinguishable results.

3. Results

[28] In this section we compare the observed solute transport with a priori predictions of the MSM-CTRW approach and the inversely estimated simulations of the TSM (section 3.1). Using the MSM, we partition the contribution of small and large topographic features to total hyporheic flow, and evaluate the sensitivity of hyporheic fluxes and residence times to variations in sediment conditions and groundwater discharge (section 3.2).

3.1. Comparison of the MSM and TSM to Solute Data

[29] Figure 3a shows the measured and predicted solute transport within the stream. Best-fit TSM parameters for the one- and two-storage-zone models are shown in Table 1. The tail of elevated tracer concentration following passage of the main pulse reflects solute that is transported through the stream reach much more slowly than the mean. The MSM prediction simulates the tail of the BTC reasonably well but does not capture the breakthrough behavior immediately after the injection stops. Thus, it appears that the MSM adequately predicted relatively long hyporheic residence times (>2 h), but not more rapid storage. The MSM model prediction does not account for in stream storage processes beyond Taylor dispersion. Although the model resolution (<1 mm) is capable of capturing very short hyporheic flow paths, its application at Sugar Creek was limited by the resolution of the topographic mapping (5 cm in the horizontal). In general, we expect it to be very difficult to represent very short and fast surface and subsurface storage processes. This is especially true on the order of several grain diameters above and below the streambed surface, because it is difficult to achieve sufficient model resolution to represent all roughness features, Darcy's law does not hold at the grain scale, and turbulent flow-boundary interactions mediate transport in this region [*Manes et al.*, 2011]. Therefore, surface and subsurface boundary layer mixing around complex stream roughness features such as cobbles and bedforms are not resolved by the MSM in its present form. To simulate such interfacial mixing, we added a fast exponentially distributed storage-exchange term (denoted EXP) to the CTRW model, equivalent to the faster of two storage zones modeled by the TSM. The parameters of this exponential storage zone were obtained by matching the OTIS 2-STOR output or fitting solute data directly. Thus, while the hyporheic residence time predictions of the MSM are truly a priori, the fast exponential portion of the breakthrough curve is not. Including this fast exponential storage captured the entire observed tail of the breakthrough curve, as shown in Figure 3.

[30] OTIS-2Stor provided a reasonable simulation of the in stream solute tracer data (Figure 3b) by allowing for fast exchange in one storage zone and slower exchange in a second storage zone. However, as these results were obtained by fitting, they cannot be explicitly linked to specific regions of the stream or subsurface. The MSM simulation that included a fast exponential storage term had a similar overall form to the TSM simulation. The major difference was that the TSM simulation reached the tracer background concentration much more quickly than did the MSM simulation, which predicted a much more extended tail. It is important to note that the uncertainty in the background concentration of the bromide tracer is larger than the difference between the simulations, especially after 27 h. This difference between the inverse and forward model simulations suggests the TSM interpretation of solute transport in Sugar Creek was limited by analytical sensitivity, as discussed by *Drummond et al.* [2012]. Further, the exponential residence time distribution

Table 1. Parameter Values for the One- and Two-Storage Zone Transport Simulations

OTIS Parameter	Description	Units	One-Storage	Two-Storage
Q	Volumetric flow rate	$m^3\ s^{-1}$	0.0406	0.0406
D	Longitudinal dispersion coefficient	$m^2\ s^{-1}$	0.06	0.3
A	Cross-sectional area (main flow zone)	m^2	0.27	0.32
q_L^{in}	Groundwater discharge	$(m^3\ s^{-1})/m$	1.1×10^{-5}	1.1×10^{-5}
A_{S1}	Cross-sectional area (storage zone 1)	m^2	0.24	0.16
A_{S2}	Cross-sectional area (storage zone 2)	m^2	–	0.03
α_1	Exchange coefficient (storage zone 1)	s^{-1}	2.5×10^{-3}	9.48×10^{-4}
α_2	Exchange coefficient (storage zone 2)	s^{-1}	–	2.54×10^{-5}
t_{S1}	Fluid residence time (storage zone 1)	s	356	527
t_{S2}	Fluid residence time (storage zone 2)	s	–	3691
Dal_{stor1}	Damkohler number (storage zone 1)	–	0.19	0.45
Dal_{stor2}	Damkohler number (storage zone 2)	–	–	0.02

implicit in the TSM formulation cannot represent extremely wide distributions of residence times, and the linear least-squares optimization in OTIS-P weights plateau and early tail observations much more than the lower concentrations found in the extended tail. As a result, the inverse modeling of solute injections with the TSM primarily captures fast exchange processes, which appear to only be a subset of the hyporheic exchange processes in Sugar Creek.

[31] Figure 4 compares cumulative residence time distributions attributed to the subsurface in the TSM and MSM. The distribution labeled OTIS-2Stor$_2$ in Figure 4 is associated with the slower of the two storage zones identified using the TSM-2Stor model. The MSM predicts a significantly broader range of exchange timescales compared with the OTIS-2Stor model. The difference in the residence time distributions results in part from the different modeling procedures, i.e., the inverse estimation procedure used for fitting the tracer breakthrough curve using OTIS-2Stor compared with the a priori predictions of the MSM based on independent physical measurements. Each model captures a different range of time scales. The TSM approach is restricted to relatively short storage timescales, approximately three times longer than the injection duration, which is the result of the exponential residence time formulation and limited tracer sensitivity. The MSM has no such limitation and thus predicts a much broader residence time distribution. The long-timescale component of hyporheic flow that TSM modeling does not resolve will generally be incorrectly accounted as loss to groundwater. Thus, TSM fits are not only likely to underestimate hyporheic residence times but also may over-estimate loss to groundwater. Conversely, the MSM provides useful predictions of hyporheic exchange on longer timescales, but its ability to predict short time scales is restricted by the spatial resolution of available topographic data and the lack of representation of the interfacial hydrodynamics. In particular, the MSM does not explicitly represent turbulent transport around bed form roughness or within pore water, which is known to be important in the uppermost part of the streambed [*Valentine and Wood*, 1977; *Salehin et al.*, 2004; *Higashino and Stefan*, 2008; *Manes et al.*, 2011]. Fast, shallow exchange processes contribute greatly to interfacial fluxes [*Wörman et al.*, 2007], which explains the substantial difference in volumetric exchange evaluated by the TSM and the MSM (Figure 4b).

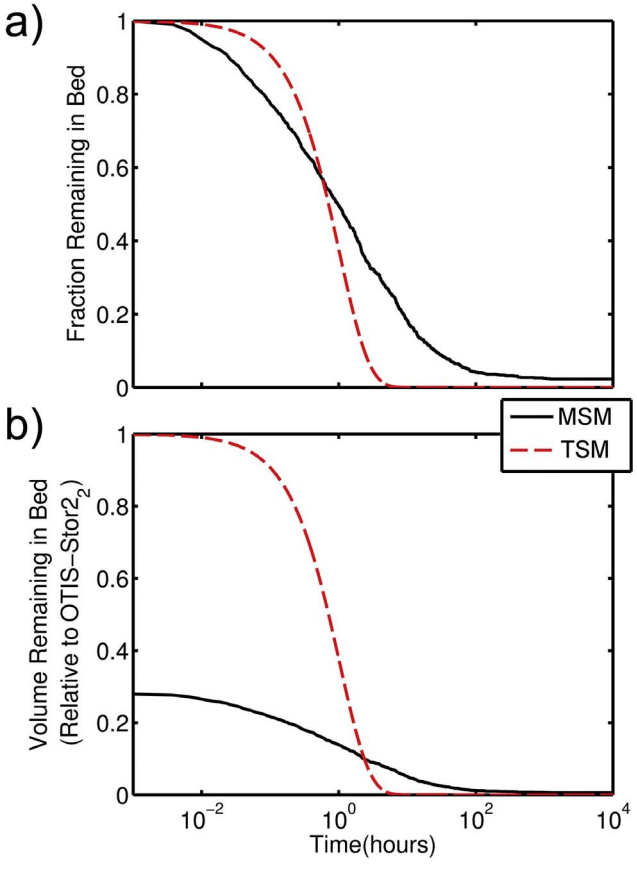

Figure 4. Residence time distributions predicted by the MSM (black line) and inferred from the slower storage compartment in the TSM model, referred to in the text as the second storage zone or OTIS-2Stor$_2$. (a) shows the fraction remaining in the bed and (b) shows the volume remaining in the bed of that which entered at time 0 relative to the OTIS-2Stor$_2$.

3.2. Exploration of Controls on Hyporheic Flow Using the MSM

[32] Many characteristics of natural streams affect patterns and rates of hyporheic exchange. One advantage of having a predictive modeling framework like the MSM is that it can be used to simulate the influence of various stream characteristics on hyporheic exchange. In this section we specifically consider how the presence or absence of small-scale streambed topography (ripples and dunes) affects hyporheic exchange. We also investigate the effects of differing groundwater discharge to the stream. For these simulations we used a hydraulic conductivity of 0.01 cm s^{-1}.

3.2.1. Interactions Between Multiple Scales of Streambed Topography

[33] Figure 5 shows the spatial distribution of simulated fluxes into and out of the sediment with both the full range of topography (ripples, dunes, bars, and meanders) and only the large-scale topography. Small-scale topography produces complex, fine-scale patterns of hyporheic exchange. The interfacial flux was 20 times greater in the simulation with full topography than in the simulation with only large-scale topography. The interfacial flux was thus dominated by small-scale topographic features, and thus occurred primarily through the streambed rather than the banks. This finding that ripple and dune features tend to dominate hyporheic exchange in the absence of substantial groundwater flows is consistent with the results obtained previously for multiscale hyporheic exchange in laboratory flumes [*Stonedahl et al.*, 2010]. In the simulations with only large topography and no groundwater discharge, the planform morphology dominates exchange and the regions of inward and outward flux are significantly less fragmented than those observed with the small topography. The hyporheic flux was greater at the narrowest sections of the stream, i.e., the areas of flow constriction where stream velocities are greatest (Figure 5). This is expected because drag over obstructions and bedforms, and thus the driving force for hyporheic flow, varies with the square of the mean stream velocity [*Elliott and Brooks*, 1997].

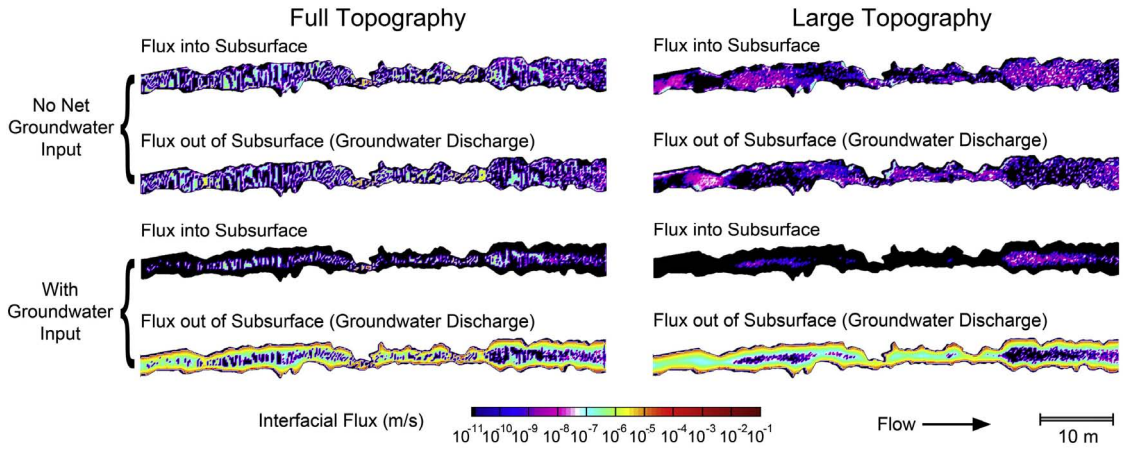

Figure 5. MSM results showing interfacial flux into and out of the subsurface for different scales of topography shown both with and without groundwater discharge.

[34] Groundwater discharge substantially reduced hyporheic exchange flux by producing an overall head gradient toward the stream. As a result, hyporheic exchange only occurred locally in areas where the head gradient into the subsurface was greater than that imposed by the groundwater inflow. Groundwater influx practically eliminated hyporheic exchange near the stream banks (Figure 5). In the simulation with the full range of topography, hyporheic exchange still occurred in a thin strip following the thalweg as a result of high head gradients induced by small topographic features. Conversely, in the simulation with only large topography, groundwater inputs restricted hyporheic exchange fluxes to only the wider sections of the stream, where groundwater inflows were distributed over a wider area. In the case with the full range of topography, the average interfacial hyporheic flux decreased from 5×10^{-7} m s^{-1} without groundwater discharge to only 1.4×10^{-7} m s^{-1} with groundwater discharge—a 73% decrease. When only large topography was considered, hyporheic exchange was even more sensitive to groundwater discharge: simulations showed an average flux into the subsurface of 2.6×10^{-8} m s^{-1} without groundwater discharge, and 1.1×10^{-9} m s^{-1} with groundwater discharge—a 96% decrease. Note that the hyporheic flux was 130x greater when the full topography was included in the simulations (with groundwater discharge). Thus, it is particularly important to account for the effects of fine-scale morphology of stream channels on hyporheic exchange in gaining stream reaches. Groundwater discharge also substantially reduced the area of the streambed where hyporheic exchange occurs. In the simulation with large topography and groundwater discharge, hyporheic flow paths originated in only 11% of the streambed, and 90% of the exchange flow occurred in only 1.7% of the streambed. Similarly, in the simulation with the full range of topography and groundwater discharge, hyporheic flow paths originated in just 17% of the streambed and 90% of the exchange flow occurred in 4.7% of the streambed.

[35] Small topographic features skew hyporheic residence time distributions toward shorter residence times, as show in Figure 6. This finding is consistent with our previous results for laboratory-generated meandering channel topography [*Stonedahl et al.*, 2010]. Groundwater discharge also decreases the residence times associated with hyporheic flow. The median residence time for hyporheic flow paths for the simulation with the full range of topography was approximately 9x smaller with groundwater discharge. Hyporheic residence times decreased even more with groundwater flow when only large topography was simulated: in this case, the median hyporheic residence time was approximately 63x smaller with groundwater discharge than without groundwater discharge.

3.2.2. Sensitivity to Groundwater Discharge

[36] We quantified the sensitivity of hyporheic flow to groundwater discharge using multiple MSM simulations with different groundwater levels assuming a constant groundwater level relative to the stream at the lateral domain boundaries. These simulations were performed with the full complexity of topography for Sugar Creek, a stream

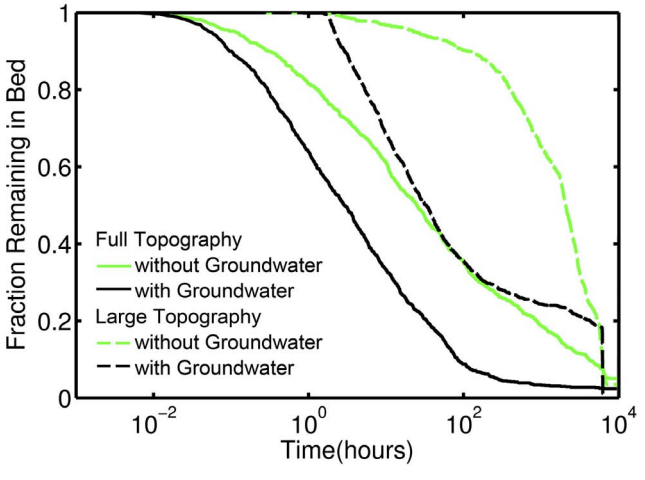

Figure 6. Flux-weighted cumulative residence time distributions of hyporheic flow from the MSM with (solid) and without (dashed) small topography. The level of groundwater discharge is indicated by as either zero (green) or at the level of groundwater discharge measured at Sugar Creek (black).

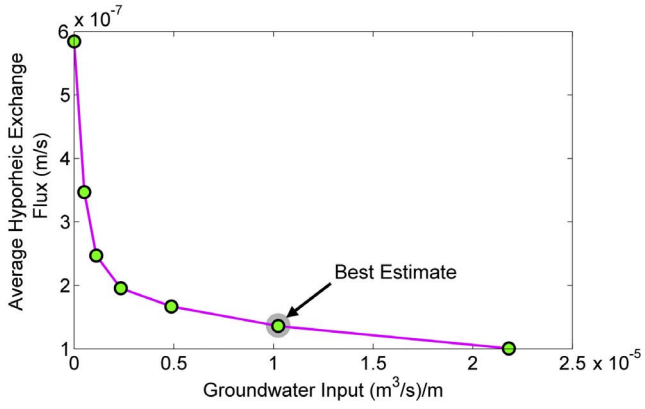

Figure 7. Simulated hyporheic exchange flux as a function of groundwater input. Hyporheic exchange decreased due to the increased groundwater discharge into the streams, as this confined the regions of flux into the subsurface.

discharge of 0.03 $m^3\ s^{-1}$, and a hydraulic conductivity of 0.01 cm s^{-1}. Results, presented in Figure 7, show a roughly hyperbolic negative relationship between groundwater discharge and hyporheic exchange. Similar relationships have been found previously [*Harvey et al.*, 1996; *Boano et al.*, 2007; *Cardenas and Wilson*, 2007]. This occurs because of the streamward head gradients associated with elevated groundwater levels. Our simulations also show that the area of streambed that contributes to hyporheic flow is decreased by greater hydraulic heads in the surrounding aquifer, as shown in Figure 5.

[37] The sensitivity of hyporheic residence times to groundwater discharge can be seen in Figure 8. The shape of the cumulative residence time distribution curves are relatively consistent with groundwater discharge. Only the simulation without groundwater discharge ($Q_{gw}/m = 0$) has hyporheic residence times that are substantially longer than the other simulations. When groundwater discharge is low, substantial hyporheic exchange occurs through the stream banks (Figure 5), and this water travels relatively long distances before returning to the stream. Higher groundwater discharge limits hyporheic flow near the banks, and instead

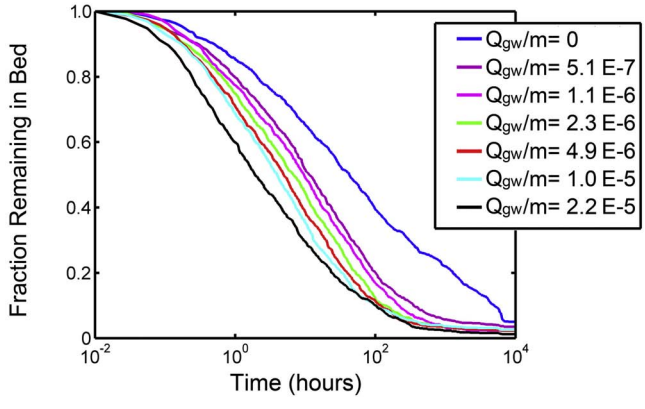

Figure 8. Flux-weighted cumulative residence time distribution for each of the groundwater sensitivity cases, where labels delineate the volumetric flux into the stream per meter ($m^3\ s^{-1}$)/m.

favors midchannel exchange, yielding shorter hyporheic flow paths and smaller residence times. Thus, in streams like Sugar Creek, even a small amount of groundwater discharge substantially reduces hyporheic residence times by changing the pattern of exchange flow.

4. Discussion and Conclusions

[38] This paper presents the first field application of our three-dimensional, predictive, MSM for hyporheic exchange [*Stonedahl et al.*, 2010]. The a priori MSM predictions of hyporheic flow were converted to predictions of in stream solute transport using the CTRW and then compared with results of a solute tracer experiment and with interpretations based on TSM model fits. In addition to extending the MSM to incorporate groundwater discharge, we developed procedures that use field stream surveys and flow measurements to calculate the boundary head distribution and streambed fluxes associated with hyporheic and groundwater flows. The results emphasize that interactions between streamflow, channel morphology, and groundwater discharge control hyporheic flow.

[39] Storage and exchange processes occur over a wide range of spatial and temporal scales in streams [*Wörman et al.*, 2007; *Cardenas*, 2008; *Stonedahl et al.*, 2010]. Transport parameters estimated by fitting in stream solute tracer data primarily reflect relatively fast exchange processes that occur within the stream itself and in shallow hyporheic flow paths. This is due largely to limitations of the tracer methodology, e.g., limited tracer sensitivity and uncertainty in tracer background concentration [*Drummond et al.*, 2012], as well as the exponential residence time formulation of the TSM. Such limitations have long been recognized [e.g., *Harvey et al.*, 1996; *Haggerty et al.*, 2002; *Gooseff et al.*, 2003]. Improved multiparameter calibrations can improve, to some degree, resolution of multiple storage zones [*Choi et al.*, 2000; *Briggs et al.*, 2009; *Neilson et al.*, 2010]. Use of multiple exponentially distributed storage zones broadens storage timescales and increases the goodness of fit of stream tracer data, especially on the extended tails of the distribution, but does not necessarily reflect discrete controlling processes or regions of solute storage. More detailed observations and more general theory are needed to fully explain observed solute transport in terms of controlling processes, and to enable a priori prediction of hyporheic exchange.

[40] The physically based MSM predicts hyporheic exchange occurring on much longer time scales than those resolved by TSM fitting of in-stream observations. Due to the limited sensitivity of traditional tracer studies, in-stream data cannot be used to evaluate the fidelity of MSM simulations of long hyporheic residence times. We found considerable uncertainty in observed tracer concentrations in the tail, as well as in the stream background concentration, even though we had fairly ideal circumstances for a tracer experiment with steady discharge and high experimental enrichment of bromide, one of the more reliable anionic tracers used in surface water. The a priori prediction of the MSM could potentially be tested with a tracer having a much greater dynamic range for in-stream observations or with long-term direct observations of the retention and wash-out of tracer from the subsurface (as employed in

Jonsson et al. [2003] and *Harvey and Fuller* [1998]). Whereas *Jonsson et al.* [2003] observed longer-term storage of tracer in the hyporheic zone than could be detected by modeling in stream transport of the tracer, *Harvey and Fuller* [1998] found that hyporheic flow matched the timescale and spatial dimension of storage detected by in stream tracer modeling. Improved sensitivity is achieved with radiotracers such as tritium [*Jonsson et al.*, 2003] or sulfur hexafluoride gas [*McCarthy et al.*, 1998], which offer orders of magnitude in dynamic range of detection. Fluorescent dyes such as Rhodamine WT also provide orders of magnitude in its dynamic range but suffer from sorption to organic matter in sediments [e.g., *Gooseff et al.*, 2003, 2005].

[41] While the MSM appeared to characterize long-term hyporheic storage better than the TSM, it did not resolve fast tracer exchange in Sugar Creek. Short tracer storage times most likely reflect both in-stream mixing, which we did not attempt to model, and fast hyporheic flow through the uppermost region of the streambed (from the top few grain diameters to the top few centimeters). The resolution of the MSM is limited by both its formulation, which involves a gross approximation of the 3-D flow-boundary interaction, and by the data available to characterize the stream. Our topographic survey had a resolution of several mm vertically, but just 5 cm horizontally, which may not have been sufficient to capture the smallest and shallowest scales of hyporheic flow. A variety of processes have been shown to induce shallow and fast hyporheic exchange, including turbulent diffusion and shallow advection induced by sediment clustering and other grain-scale phenomena [*Packman et al.*, 2004; *Higashino and Stefan*, 2008; *O'Connor and Harvey*, 2008; *Grant and Marusic*, 2011]. The addition of an exponential storage/exchange term representing these short residence times greatly improved the comparison between the observations and predictions. However, no method currently exists to independently predict near-boundary mixing and grain-scale exchange, and so this fast exponential exchange term could only be obtained by fitting solute data.

[42] Additional effort should be expended to characterize both surface water mixing processes and fast hyporheic mixing processes. *O'Connor et al.* [2010] found that tracer experiments typically detect relatively fast exchange between the main channel and surface water storage zones, and that transport parameters were predictable based on statistical relationships developed using data from many previous tracer experiments (e.g., storage zone size scales with friction factor). Typically all that is required are physical measurements of streambed slope, average channel width and depth, and average streamflow velocity. Bedform-scale topography is frequently not measured or considered in solute transport studies, however, especially those that focus on biological or ecological processes. This is problematic because such features tremendously impact current-driven hyporheic exchange and often dominate surface-subsurface water fluxes [*Boano et al.*, 2007; *Cardenas and Wilson*, 2007; *Stonedahl et al.*, 2010]. Accurate prediction of fast, near-surface hyporheic exchange dominated by bedforms is important because many biological processes exhibit very high rates just at and around the streambed surface, where photosynthesis supports strong algal activity and stimulates aerobic bacterial metabolism [e.g., *O'Connor and Harvey*, 2008; *O'Connor et al.*, 2012]. It is also extremely important to separate surface and subsurface mixing processes that have similar transport timescales because transformation and uptake rates of most chemically and biologically active solutes differ tremendously between the water column and underlying sediments [*Dahm and Valett*, 1996; *Harvey and Fuller*, 1998; *Jones and Mulholland*, 2000; *Arnon et al.*, 2007]. Initial estimates of bedform-scale exchange can be obtained using the scaling laws developed by *O'Connor and Harvey* [2008] or a two-dimensional pumping model like *Elliott and Brooks* [1997]. Here we found that including dune- and ripple-scale topography both increased hyporheic flux and decreased the median hyporheic residence time by an order of magnitude in the absence of groundwater discharge, and by 2 orders of magnitude in the presence of groundwater discharge.

[43] We also found that groundwater discharge significantly impacts both rates and patterns of hyporheic exchange. MSM simulations indicate that the average hyporheic flux in Sugar Creek decreased approximately by a factor of four under the measured groundwater discharge (1.1×10^{-5} (m^3 s^{-1})/m) relative to the case with no groundwater discharge. Similar decreases in interfacial flux with groundwater inflow have been observed both in the field [*Harvey et al.*, 1996] and in prior model simulations [*Cardenas and Wilson*, 2006; *Cardenas and Wilson*, 2007; *Boano et al.*, 2009]. Our simulations suggest that hyporheic exchange is very sensitive to small amounts of groundwater discharge, but there is a threshold above which hyporheic fluxes are relatively insensitive to further changes in groundwater discharge. In the case of Sugar Creek, we found that hyporheic exchange rates became less sensitive to groundwater inputs when the ratio of groundwater influx to the hyporheic exchange flux without groundwater was greater than two. Specifically at $Q_{gw}/Q_{hyporheic} = 2$, a further doubling of the groundwater discharge only decreased hyporheic exchange flux by 15%. There is no reason to believe this threshold will be universal. Recently, *Bhaskar et al.* [2012] used numerical modeling results of *Cardenas and Wilson* [2007] to show that bed form-scale hyporheic flow is insensitive until groundwater fluxes exceed hyporheic fluxes by several orders of magnitude. Unlike the present work the latter study only considered two dimensional flow and did not consider concentrated groundwater discharge at banks or a confining layer beneath the stream. Although both studies are consistent in describing thresholds, the very different results suggest a need for more research on groundwater and hyporheic interactions.

[44] The high sensitivity of hyporheic flow patterns and rates to low levels of groundwater discharge makes it extremely important to characterize groundwater discharge in all field solute transport studies. A similar recommendation was made recently by *Bencala et al.* [2011]. These findings pose a challenge for field observation since considerably different methods must be used to characterize groundwater flow, surface water flow, stream morphology, and hyporheic exchange. We obtained our estimates of groundwater inflow from tracer dilution during the solute injection, but this does not provide information on the spatial variability of groundwater inputs to the stream channel. More extensive measurement of groundwater involves

inserting piezometers in and around the stream [*Wroblicky et al.*, 1998]. This method would have been difficult at Sugar Creek because the banks are very steep and the groundwater level is several meters below the ground surface. Even at field sites well suited for piezometers, large numbers of measurements are generally needed to adequately characterize the groundwater flow field. Tracers can be used to estimate groundwater discharge [*Kimball et al.*, 2002; *Payn et al.*, 2009], but it is difficult to distinguish between groundwater discharge and long hyporheic flow paths [*Bencala et al.*, 2011]. As a result, groundwater levels around streams are frequently poorly characterized, and most studies of hyporheic exchange neglect groundwater discharge and its effects on hyporheic flow entirely. We found that hyporheic exchange was most sensitive to low levels of groundwater discharge, indicating that groundwater interactions should be characterized even when they are expected to be small.

[45] Finally, we highlight the benefits of using an ensemble of theoretical and empirical methods to increase understanding of the processes that control hyporheic flow and improve prediction of the net effects of hyporheic exchange. Hyporheic exchange has most commonly been inferred from stream tracer experiments and inverse modeling, but there is increasing recognition that those methods do not adequately characterize the full rates, timescales, and distributions of exchange. Conversely, our MSM provides a means to characterize both patterns of hyporheic exchange flow and the extended exchange timescales that result from interactions between surface and groundwaters over a wide range of spatial scales. The MSM requires only relatively simple measurements: stream bathymetry, streamflow conditions, an average hydraulic conductivity for the subsurface, and an estimate of groundwater discharge. Subsurface heterogeneity can also be included, if data are available to characterize it. With these inputs, the model can be used to generate a priori estimates of hyporheic fluxes and flowpaths over multiple scales, and to perform sensitivity analyses of the effects of various exchange mechanisms. However, the resolution of such models is currently limited by a lack of knowledge of turbulent interactions with porewaters, computational cost for highly detailed three-dimensional simulations of turbulent flows over complex boundaries, and the difficulty of obtaining sufficiently detailed field data.

[46] In the field application here, we showed the sensitivity of hyporheic flow to channel morphology, streambed roughness, and groundwater discharge in a heavily manipulated Midwestern agricultural stream, where hyporheic flow is known to substantially influence nitrogen export [*Böhlke et al.*, 2009; *Alexander et al.*, 2009]. Given the limitations of all available approaches to characterizing hyporheic exchange, we believe that a blend of experimental, inverse, and predictive modeling approaches must be used to interpret exchange behavior over the range of scales relevant to stream biogeochemistry, as well as to provide the information needed to manage water resources and aquatic ecosystems.

[47] **Acknowledgments.** This work was supported by the U.S. National Science Foundation grants HS-0408744 and HS-0810140 and by the U.S. Geological Survey's HR&D and NAWQA programs. Computational resources were provided by Northwestern's Quest HPCC. We thank Lisa Marx, Boris Lau, and Stan Mroczkowski for assistance in field measurements and Forrest Stonedahl for python scripting which automated the MATLAB-Modflow interface. We thank Ken Bencala, Audrey Sawyer, Roy Haggerty, Mike Gooseff, and Bayani Cardenas for their insightful comments on the manuscript. Any use of trade, firm, or product names is for descriptive purposes only and does not imply endorsement by the U.S. Government.

References

Alexander, R. B., et al. (2009), Dynamic modeling of nitrogen losses in river networks unravels the coupled effects of hydrological and biogeochemical processes, *Biogeochemistry*, *93*(1–2), 91–116, doi:10.1007/s10533-008-9274-8.

Arnon, S., K. A. Gray, and A. I. Packman (2007), Biophysicochemical process coupling controls nitrate use by benthic biofilms, *Limnol. Oceanogr.*, *52*(4), 1665–1671, doi:10.4319/lo.2007.52.4.1665.

Bencala, K. E., and R. A. Walters (1983), Simulation of solute transport in a mountain pool-and-riffle stream: A transient storage model, *Water Resour. Res.*, *19*(3), 718–724.

Bencala, K. E., M. N. Gooseff, and B. A. Kimball (2011), Rethinking hyporheic flow and transient storage to advance understanding of stream-catchment connections, *Water Resour. Res.*, *47*, W00H03, doi:10.1029/2010WR010066.

Benner, S. G., E. W. Smart, and J. N. Moore (1995), Metal behavior during surface-groundwater interaction, Silver Bow Creek, Montana, *Environ. Sci. Technol.*, *29*(7), 1789–1795.

Berkowitz, B., A. Cortis, M. Dentz, and H. Scher (2006), Modeling non-Fickian transport in geological formations as a continuous time random walk, *Rev. Geophys.*, *44*, RG2003, doi:10.1029/2005RG000178.

Beven, K., and A. Binley (1992), The future of distributed models: Model calibration and predictive uncertainty, *Hydrol. Processes*, *6*(3), 279–298.

Bhaskar, A. S., J. W. Harvey, and E. J. Henry (2012), Resolving hyporheic and groundwater components of streambed water flux using heat as a tracer, *Water Resour. Res.*, *48*, W08524, doi:10.1029/2011WR011784.

Boano, F., A. I. Packman, A. Cortis, R. Revelli, and L. Ridolfi (2007), A continuous time random walk approach to the stream transport of solutes, *Water Resour. Res.*, *43*,W10425, doi:10.1029/2007WR006062.

Boano, F., R. Revelli, and L. Ridolfi (2009), Quantifying the impact of groundwater discharge on the surface-subsurface exchange, *Hydrol. Processes*, *23*, 2108–2116, doi:10.1002/hyp.7278.

Böhlke, J. K., J. W. Harvey, and M. A. Voytek (2004), Reach-scale isotope tracer experiment to quantify denitrification and related processes in a nitrate-rich stream, midcontinent United States, *Limnol. Oceanogr.*, *49*(3), 821–838.

Böhlke, J. K., R. C. Antweiler, J. W. Harvey, A. E. Laursen, L. K. Smith, R. L. Smith, and M. A. Voytek (2009), Multi-scale measurements and modeling of denitrification in streams with varying flow and nitrate concentration in the upper Mississippi River basin, USA, *Biogeochemistry*, *93*, 117–141, doi:10.1007/s10533-008-9282-8.

Briggs, M. A., M. N. Gooseff, C. D. Arp, and M. A. Baker (2009), A method for estimating surface transient storage parameters for streams with concurrent hyporheic storage, *Water Resour. Res.*, *45*, W00D27, doi:10.1029/2008WR006959, [printed 46(4), 2010].

Cardenas, M. B. (2008), Surface water-groundwater interface geomorphology leads to scaling of residence times, *Geophys. Res. Lett.*, *35*, L08402, doi:10.1029/2008GL033753.

Cardenas, M. B. (2009a), Stream-aquifer interactions and hyporheic exchange in gaining and losing sinuous streams, *Water Resour. Res.*, *45*(6), W06429, doi:10.1029/2008WR007651.

Cardenas, M. B. (2009b), A model for lateral hyporheic flow based on valley slope and channel sinuosity, *Water Resour. Res.*, *45*(1), W01501, doi:10.1029/2008WR007442.

Cardenas, M. B., and J. L. Wilson (2006), The influence of ambient groundwater discharge on exchange zones induced by current-bedform interactions, *J. Hydrol.*, *331*(1–2), 103–109, doi:10.1016/j.jhydrol.2006.05.012.

Cardenas, M. B., and J. L. Wilson (2007), Dunes, turbulent eddies, and interfacial exchange with permeable sediments, *Water Resour. Res.*, *43*, W08412, doi:10.1029/2006WR005787.

Cardenas, M. B., J. L. Wilson, and R. Haggerty (2008), Residence time of bedform-driven hyporheic exchange, *Adv. Water Resour.*, *31*(10), 1382–1386, doi:10.1016/j.advwatres.2008.07.006.

Choi, J., J. W. Harvey, and M. H. Conklin (2000), Characterizing multiple timescales of stream and storage zone interaction that affect solute fate and transport in streams, *Water Resour. Res.*, *36*(6), 1511–1518, doi:10.1029/2000WR900051.

Cortis, A., and B. Berkowitz (2005), Computing "anomalous" contaminant transport in porous media: The CTRW MATLAB Toolbox, *Ground Water*, *43*(6), 947–950.

Dahm, C. N., and H. M. Valett (1996), Hyporheic Zones, in *Methods in Stream Ecology*, edited by F. R. Hauer and G. A. Lamberti, pp. 107–122, Academic Press, San Diego, Calif.

Dentz, M., and B. Berkowitz (2003), Transport behavior of a passive solute in continuous time random walks and multirate mass transfer, *Water Resour. Res.*, *39*(5), 1111, doi:10.1029/2001WR001163.

De Hoog, F. R., J. H. Knight, and A. N. Stokes (1982), An improved method for numerical inversion of Laplace transforms, *SIAM J. Sci. Stat. Comput.*, *3*, 357–366.

Driscoll, T. A. (1996), Algorithm 756: A MATLAB toolbox for Schwarz-Christoffel mapping, *ACM Trans. Math. Software*, *22*(2), 168–186.

Drummond, J. D., T. P. Covino, A. F. Aubeneau, D. Leong, S. Patil, R. Schumer, and A. I. Packman (2012), Effects of solute breakthrough curve tail truncation on residence time estimates: A synthesis of solute tracer injection studies, *J. Geophys. Res.*, *117*, G00N08, doi:10.1029/2012JG002019.

Elliott, A. H., and N. H. Brooks (1997), Transfer of nonsorbing solutes to a streambed with bed forms: Theory, *Water Resour. Res.*, *33*(1), 123–136.

Fehlman, H. M. (1985), Resistance components and velocity distributions of open channel flows over bedforms, Masters' thesis, Colo. State Univ., Fort Collins, Colo.

Fischer, H. B., E. J. List, R. C. Koh, J. Imberger, and N. H. Brooks (1979), *Mixing in Inland and Coastal Waters*, 483 pp., Academic, San Diego, Calif.

Fuller, C. C., and J. W. Harvey (2000), Reactive uptake of trace metals in the hyporheic zone of a mining-contaminated stream, Pinal Creek, AZ, *Environ. Sci. Technol.*, *34*, 1150–1155, doi:10.1021/es990714d.

Gooseff, M. N., S. M. Wondzell, R. Haggerty, and J. Anderson (2003), Comparing transient storage modeling and residence time distribution (RTD) analysis in geomorphically varied reaches in the Lookout Creek basin, Oregon, USA, *Adv. Water Resour.*, *26*(9), 925–937.

Gooseff, M. N., K. E. Bencala, D. T. Scott, R. L. Runkel, and D. M. McKnight (2005), Sensitivity analysis of conservative and reactive stream transient storage models applied to field data from multiple-reach experiments, *Adv. Water Resour.*, *28*(5), 479–492, doi:10.1016/j.advwatres.2004.11.012.

Grant, S. B., and I. Marusic (2011) Crossing turbulent boundaries: Interfacial flux in environmental flows, *Environ. Sci. Technol.*, *45*, 7107–7113, doi:10.1021/es201778s.

Haggerty, R., S. M. Wondzell, and M. A. Johnson (2002) Power-law residence time distribution in the hyporheic zone of a 2nd-order mountain stream, *Geophys. Res. Lett.*, *29*(13), 1640, doi:10.1029/2002GL014743.

Harbaugh, A. W., E. R. Banta, M. C. Hill, and M. G. McDonald (2000), MODFLOW-2000, the U.S. Geological Survey modular ground-water model—User guide to modularization concepts and the ground-water flow process, *U.S. Geol. Surv. Open-File Rep. 00-92*, 1–21.

Harvey, J. W., and K. E. Bencala (1993), The effect of streambed topography on surface-subsurface water exchange in mountain catchments, *Water Resour. Res.*, *29*(1), 89–98.

Harvey, J. W., and C. C. Fuller (1998), Effect of enhanced manganese oxidation in the hyporheic zone on basin-scale geochemical mass balance, *Water Resour. Res.*, *34*(4), 623–636.

Harvey, J. W., and B. J. Wagner (2000), Quantifying hydrologic interactions between streams and their subsurface hyporheic zones, in *Streams and Groundwaters*, edited by J. B. Jones and P. J. Mulholland, pp. 3–44, Academic Press, San Diego, Calif.

Harvey, J. W., J. E. Saiers, and J. T. Newlin (2005), Solute transport and storage mechanisms in wetlands of the Everglades, south Florida, *Water Resour. Res.*, *41*, W05009, doi:10.1029/2004WR003507.

Harvey, J. W., B. J. Wagner, and K. E. Bencala (1996), Evaluating the reliability of the stream tracer approach to characterize stream-subsurface water exchange, *Water Resour. Res.*, *32*(8), 2441–2451.

Harvey, J. W., M. H. Conklin, R. S. Koelsch (2003), Predicting changes in hydrologic retention in an evolving semi-arid alluvial stream, *Adv. Water Resour.*, *26*(9), 939–950, doi:10.1016/s0309-1708(03)00085-x.

Higashino, M., and H. G. Stefan (2008), Near-bed turbulence models: Significance for diffusional mass transfer at the sediment/water interface, *J. Hydraul. Res.*, *46*(3), 291–300, doi:10.3826/jhr.2008.2769.

Hvorslev, M. (1951), Time lag and soil permeability in ground-water observations, edited, *U.S. Army Waterways Exper. Station Bull. 36*, U.S. Army Corps of Engineers, Vicksburg, Miss.

Jones, J. B., and P. J. Mulholland (Eds.) (2000), *Streams and Groundwaters*, Academic Press, San Diego, Calif.

Jonsson, K., H. Johansson, and A. Wörman (2003), Hyporheic exchange of reactive and conservative solutes in streams-tracer methodology and model interpretation, *J. Hydrol.*, *278*(1–4), 153–171, doi:10.1016/S0022169 4(03)00140-9.

Kimball, B. A., R. L. Runkel, K. Walton-Day, K. E. Bencala (2002), Assessment of metal loads in watersheds affected by acid mine drainage by using tracer injection and synoptic sampling: Cement Creek, Colorado, USA, *Appl. Geochem.*, *17*, 1183–1207, doi:10.1016/S0883-2927(02)00017-3.

Landon, M. K., D. L. Rus, and F. E. Harvey (2001), Comparison of instream methods for measuring hydraulic conductivity in sandy streambeds, *Ground Water*, *39*(6), 870–885, doi:10.1111/j.1745-6584.2001.tb02475.x.

Larkin, R. G., and J. M. Sharp Jr. (1992), On the relationship between river-basin geomorphology, aquifer hydraulics and groundwater flow direction in alluvial aquifers, *Geol. Soc. Am. Bull.*, *104*(12), 1608–1620.

Manes, C., D. Poggi, and L. Ridolfi (2011), Turbulent boundary layers over permeable walls: Scaling and near-wall structure, *J. Fluid Mech.*, *687*, 1–30, doi:10.1017/jfm.2011.329.

McCarthy, J. F., W. E. Sanford, and P. L. Stafford (1998), Lanthanide field tracers demonstrate enhanced transport of transuranic radionuclides by natural organic matter, *Environ. Sci. Technol.*, *32*(24), 3901–3906, doi:10.1021/es971004f.

McKnight, D. M., E. W. Boyer, P. K. Westerhoff, P. T. Doran, T. Kulbe, and D. T. Andersen (2001), Spectrofluorometric characterization of dissolved organic matter for indication of precursor organic material and aromaticity, *Limnol. Oceanogr.*, *46*(1), 38–48, doi:10.4319/lo.2001.46.1.0038.

Medina, M. A., R. L. Doneker, N. Grosso, D. M. Johns, W. Lung, M. F. N. Mohsen, A. I. Packman, and P. J. Roberts (2002), Surface water–ground water interactions and modeling applications, in *Environmental Modeling and Management: Theory, Practice and Future Directions*, edited by, C. C. Chien et al., pp. 1–62, DuPont Company, Wilmington, Del.

Metzler, R., and J. Klafter (2000), The random walk's guide to anomalous diffusion: A fractional dynamics approach, *Phys. Rep.*, *339*(1), 1–77, doi:10.1016/S0370-1573(00)00070-3.

Montroll, E. W., and G. H. Weiss (1965), Random walks on lattices. II., *J. Math. Phys.*, *6*(2), 167–181, doi:10.1063/1.1704269.

Mulholland, P. J., E. R. Marzolf, J. R. Webster, and D. R. Hart (1997), Evidence that hyporheic zones increase heterotrophic metabolism and phosphorus uptake in forest streams, *Limnol. Oceanogr.*, *42*(3), 443–451.

Neilson, B. T., D. K. Stevens, S. C. Chapra, and C. Bandaragoda (2010), Two-zone transient storage modeling using temperature and solute data with multiobjective calibration: 2. Temperature and solute, *Water Resour. Res.*, *46*, W12521, doi:10.1029/2009WR008759.

O'Connor, B. L., and J. W. Harvey (2008), Scaling hyporheic exchange and its influence on biogeochemical reactions in aquatic ecosystems, *Water Resour. Res.*, *44*,W12423, doi:10.1029/2008WR007160.

O'Connor, B. L., M. Hondzo, and J. W. Harvey (2010), Predictive Modeling of Transient Storage and Nutrient Uptake: Implications for Stream Restoration, *Journal of Hydraulic Engineering-Asce*, *136*(12), 1018–1032, doi:10.1061/(asce)hy.1943-7900.0000180.

O'Connor, B. L., J. W. Harvey, and L. E. McPhillips (2012), Thresholds of flow-induced bed disturbances and their effects on stream metabolism in an agricultural river, *Water Resour. Res.*, *48*, W08504, doi:10.1029/2011WR011488.

Packman, A. I., and K. E. Bencala (2000), Modeling methods in the study of surface-subsurface hydrologic interactions, in *Streams and Groundwaters*, edited by J. B. Jones and P. J. Mulholland, pp. 45–80, Academic Press, San Diego, Calif.

Packman, A. I., and N. H. Brooks (2001), Hyporheic exchange of solutes and colloids with moving bed forms, *Water Resour. Res.*, *37*(10), 2591–2605, doi:10.1029/2001WR000477.

Packman, A. I., M. Salehin, and M. Zaramella (2004), Hyporheic exchange with gravel beds: Basic hydrodynamic interactions and bedform-induced advective flows, *J. Hydraul. Eng.*, *130*(7), 647–656, doi:10.1061/(asce)0733-9429(2004)130:7(647).

Payn, R. A., M. N. Gooseff, B. L. McGlynn, K. E. Bencala, and S. M. Wondzell (2009), Channel water balance and exchange with subsurface flow along a mountain headwater stream in Montana, United States, *Water Resour. Res.*, *45*, W11427, doi:10.1029/2008WR007644.

Reynolds, W. D., D. E. Elrick, and E. G. Youngs (2002), Ring or cylinder infiltrometers, in *Methods of Soil Analysis Part 4 Physical Methods*, edited by J. H. Dane and G. C. Topp, Soil Sci. Soc. Am., Madison, Wisc.

Runkel, R. L. (1998), One-dimensional transport with inflow and storage (OTIS): A solute transport model for streams and rivers, *U.S. Geol. Surv. Water-Resour. Invest. Rep. 98-4018*, 73 p.

Salehin, M., A. I. Packman, and A. Wörman (2003), Comparison of transient storage in vegetated and unvegetated reaches of a small agricultural stream in Sweden: Seasonal variation and anthropogenic manipulation, *Adv. Water Resour.*, *26*(9), 951–964.

Salehin, M., A. I. Packman, and M. Paradis (2004), Hyporheic exchange with heterogeneous streambeds: Laboratory experiments and modeling, *Water Resour. Res.*, *40*(11), W11504, doi:10.1029/2003WR002567.

Schumer, R., D. A. Benson, M. M. Meerschaert, and B. Baeumer (2003), Fractal mobile/immobile solute transport, *Water Resour. Res.*, *39*(10), 1296, doi:10.1029/2003WR002141.

Smith, L. K., M. A. Voytek, J. K. Böhlke, and J. W. Harvey (2006), Denitrification in nitrate-rich streams: Application of N2: Ar and 15N-tracer methods in intact cores, *Ecol. Appl.*, *16*(6), 2191–2207, doi:10.1890/1051-0761(2006)016[2191:DINSAO]2.0.CO;2.

Stonedahl, S. H., J. W. Harvey, A. Wörman, M. Salehin, and A. I. Packman (2010), A multi-scale model for integrating hyporheic exchange from ripples to meanders, *Water Resour. Res.*, *46*, W12539, doi:10.1029/2009WR008865.

Storey, R., K. Howard, and D. Williams (2003), Factors controlling riffle-scale hyporheic exchange flows and their seasonal changes in a gaining stream: A three-dimensional groundwater flow model, *Water Resour. Res.*, *39*(2), 1034, doi:10.1029/2002WR001367.

Stream Solute Workshop (1990), Concepts and methods for assessing solute dynamics in stream ecosystems, *J. North Am. Benthological Soc.*, *9*(2), 95–119.

Taylor, G. I. (1953), Dispersion of soluble matter in solvent flowing slowly through a tube, *Proc. Roy. Soc. A.*, *219*, 186–203.

Thibodeaux, L. J., and J. D. Boyle (1987), Bedform-generated convective transport in bottom sediment, *Nature*, *325*(6102), 341–343.

Tobias, C., J. K. Böhlke, and J. W. Harvey (2007), The oxygen-18 isotope approach for measuring aquatic metabolism in high productivity waters, *Limnol. Oceanogr.*, *52*(4), 1439, doi:10.4319/lo.2007.52.4.1439.

Triska, F. J., J. H. Duff, and R. J. Avanzino (1993), The role of water exchange between a stream channel and its hyporheic zone in nitrogen cycling at the terrestrial-aquatic interface, *Hydrobiologia*, *251*(1–3), 167–184.

Valentine, E. M., and I. R. Wood (1977), Longitudinal dispersion with dead zones, *J. Hydraul. Div.*, *103*(9), 975–990.

Valett, H. M., J. A. Morrice, C. N. Dahm, and M. E. Campana (1996), Parent lithology, surface-groundwater exchange, and nitrate retention in headwater streams, *Limnol. Oceanogr.*, *41*(2), 333–345.

Williams, D. D., and H. B. N. Hynes (1974), The occurrence of benthos deep in the substratum of a stream, *Freshwater Biol.*, *4*(3), 233–256, doi:10.1111/j.1365-2427.1974.tb0009.

Wondzell, S. M., and F. J. Swanson (1996), Seasonal and storm dynamics of the hyporheic zone of a 4th-order mountain stream. 1. Hydrologic processes, *J. North Am. Benthol. Soc.*, *15*(1), 3–19.

Wörman, A., A. I. Packman, L. Marklund, J. W. Harvey, and S. H. Stone (2007), Fractal topography and subsurface water flows from fluvial bedforms to the continental shield, *Geophys. Res. Lett.*, *34*(7), L07402, doi:10.1029/2007GL029426.

Wroblicky, G. J., M. E. Campana, H. M. Valett, and C. N. Dahm (1998), Seasonal variation in surface-subsurface water exchange and lateral hyporheic area of two stream-aquifer systems, *Water Resour. Res.*, *34*(3), 317–328.